Geological Quarterly, 2025, 69, 8
DOI: https://dx.doi.org/10.7306/gq.1781

The use of microtextural and arsenic markers in the study of pyrite framboids and microcrystals

Zdzisław M. MIGASZEWSKI[1, *], Agnieszka GAŁUSZKA[1], Andrzej MIGASZEWSKI[2] and Grzegorz ZIELIŃSKI[3]

[1] Jan Kochanowski University, Uniwersytecka 7, 25-406 Kielce, Poland; ORCID: 0000-0001-5549-6224 [Z.M.M.] 0000-0002-2497-2627 [A.G.]

[2] Kielce University of Technology, Faculty of Environmental Engineering, Geomatics and Renewable Energy, Domaszowska 7, 25-314 Kielce, Poland; ORCID: 0000-0002-9215-9742

[3] Polish Geological Institute – National Research Institute, Rakowiecka 4, 00-975 Warszawa, Poland, ORCID: 0000-0001-7707-1673

Migaszewski, Z.M., Gałuszka, A., Migaszewski, A., Zieliński, G., 2025. The use of microtextural and arsenic markers in the study of pyrite framboids and microcrystals. Geological Quarterly, **69**, 8; https://doi.org/10.7306/gq.1781

Associate Editor: Tomasz Bajda

We characterize the morphology and arsenic contents of pyrite framboids *versus* pyrite microcrystals in the Upper Cambrian pyrite stratiform deposit of the Wiśniówka area (south-central Poland). The framboids form isolated spherical or ellipsoidal aggregates varying from 4 to 70 μm across or irregular agglomerations (polyframboidal aggregations) attaining 150 μm in size. Each of them is made up of loosely- or closely-packed, equidimensional, equimorphic, locally multifaceted nano- and microcrystallites (nano- and microglobules) ranging mostly from tens of nanometres to 1.5 μm in diameter. Some framboids show a well-preserved pyritized spider-web-like matrix (organic biofilm) with embedded pyrite crystallites. Unlike pyrite microcrystals, framboids lack mineral inclusions and do not form paragenetic associations with hydrothermal index minerals. Some corroded framboids are completely overgrown by pyrite microcrystals averaging 10–15 μm in diameter. In contrast to pyrite microcrystals enriched in As (0.06–6.33 wt.%), framboid occurrences are distinctly depleted in this metalloid which varies from <0.015 to 0.43 wt.% in recrystallized forms of primary framboids. In pyrite framboids cobalt usually predominates over nickel (with a Co/Ni median ratio of ~3) as opposed to pyrite microcrystals in which cobalt is barely traceable. This study indirectly shows that framboids represent products of microbial activity presumably as low-temperature bacterial sulphate reduction. Their formation may have preceded high-temperature multi-stage influxes of metal(loid)- and H_2S-rich hydrothermal fluids into the depositional basin giving rise to crystallization of pyrite microcrystals and their aggregations that vary from tens to hundreds of micrometres in diameter. This pyrite type prevails over framboids in the upper parts of the Podwiśniówka-Wiśniówka Duża profile. The morphological, microtextural and geochemical relationships between pyrite framboids and pyrite microcrystals suggest two different pathways of pyrite formation.

Key words: pyrite stratiform deposit, framboids, pyrite microcrystals, arsenic, microtextures.

INTRODUCTION

Framboids resemble raspberry-shaped spherical aggregates, and their name comes from the French word “framboise” (Rust, 1935). Each framboid comprises multifaceted nano- to microcrystallites composed mostly of pyrite, occasionally of magnetite, hematite, arsenopyrite, sphalerite, galena, etc. (Sawłowicz, 1993, 2000 and references therein). Pyrite framboids occur in a variety of reducing sedimentary or metasedimentary settings, e.g., dark grey to black muds, mudstones, clayey shales, tills, carbonates, coals, as well as soils, tailings piles or some hydrothermal veins ranging from the Precambrian to the present time in age (e.g., Ostwald and England, 1979; Wilkin and Barnes, 1997; Butler and Rickard, 2000; Paktunc and Davé, 2002; Lowers et al., 2007; MacLean et al., 2008; Soliman and El Goresy, 2012; Sugawara et al., 2013; Kamata and Katoh, 2019; Ueshima et al., 2019; Mukherjee et al., 2020; Itaya, 2022). Interestingly, submicrometre-sized pyrite framboid

* Corresponding author, e-mail: zmig@ujk.edu.pl
Received: September 13, 2024; accepted: March 13, 2025; first published online: May 21, 2025

spherules attaining 140 μm in diameter have also been found on the pages of Renaissance manuscripts (16th–17th centuries) at the Archivo Histórico Nacional in Madrid (Spain). The source of iron and sulphur was the ink containing tannin mixed with iron sulphate, whereas carbon and nitrogen came from cellulose and arabic gum (Garcia-Guinea et al., 1997).

Despite widespread occurrences of framboidal pyrite, its origin has aroused many controversies among scientists. The pivotal issue of this dispute is their inorganic or organic formation. Some researchers point to bacterially-induced processes that take place in organic-rich sedimentary environments at a temperature of ~25°C (e.g., Schopf, 1965; Folk, 1993, 2005; Schieber, 2002; Astafieva et al., 2005; Gong et al., 2008; Cavalazzi et al., 2014), whereas others indicate an inorganic pathway of pyrite framboid formation (e.g., Sawłowicz, 1993; Wilkin et al., 1996; Wilkin and Barnes, 1997; Mozer, 2010; Wang et al., 2013; Gregory et al., 2014, 2022; Smolarek et al., 2014; Działak et al., 2022; Cai et al., 2024). Experimental data indicate that inorganic framboids may form in hydrothermal systems at a temperature range of 150 to at least 350°C (Graham and Ohmoto, 1994). There is also a lack of agreement about the mechanisms that lead to the growth and aggregation of crystallites (Ohfuji and Rickard, 2005). For example, Sawłowicz (1993) proposed three inorganic pathways of pyrite framboid generation:

- indirect formation through iron monosulphides into individual globules;
- direct precipitation from solution in the form of euhedra;
- continuous growth from iron monosulphide globules to euhedral grains.

Compared to pyrite microcrystals, framboidal nano- and microcrystallites undergo a more rapid nucleation and growth rate under supersaturated conditions induced by increased Eh (Ohfuji and Rickard, 2005).

Sedimentary pyrite has not been given much attention as a source of microbial fossils. Studies have shown that both early diagenetic chert and the more common pyrite may be the best media for preserving microfossil remains (Schopf, 1965; Schieber, 2002). Hence, framboids may be used as a biomarker in the search for life in palaeoenvironmental systems on Earth and other planets (Schieber 2002; Popa et al., 2004; Gong et al., 2008; MacLean et al., 2008). Pyrite framboids have also been found, for example, in fossil chambers of pyritized radiolarian skeletons (Szczepanik et al., 2004) and in shells of living bivalves (Clark and Lutz, 1980), which may be indicative of their organic provenance.

Studies by other researchers have been focused on different sedimentary and diagenetic transformations of framboidal pyrite with no indication of its provenance (e.g., Love, 1971; Chang et al., 2022). Measurements of pyrite framboid diameter and width of size distribution range have also been used as a proxy for reconstruction of palaeoredox conditions in mudrocks. Wilkin et al. (1996) divided framboids into two groups: (i) syngenetic (<6 μm across) formed under euxinic/anoxic (lack of O_2 and H_2S abundance/lack of both O_2 and H_2S) conditions, and (ii) diagenetic (≥7 μm in size) originated in dysoxic/oxic (low O_2/high O_2 contents) conditions. Many textural, mineralogical and geochemical aspects of framboid formation were summarized by Rickard (2021).

More recent investigations of pyrite framboids have also been centred on hydrothermal vent environments involving determinations of trace elements and stable sulphur isotopes (Zhang J. et al., 2011; Hu et al., 2022; Liu et al., 2022; Zhang W.D. et al., 2022). A study by Zhang W.D. et al. (2022) suggests that negative stable sulphur isotope signatures of framboidal pyrite indicate bacterial sulphate reduction (BSR), whereas their positive values are linked to thermochemical sulphate reduction (TSR). Framboidal pyrite clusters may also show large variations in ^{34}S values, for instance from –27 to –13‰ in BSR pyrite from the Devonian Nisku Formation, Alberta, Canada (Machel, 2001).

The 2014–2023 acid mine drainage studies that were conducted in the Wiśniówka massif also encompassed the mineralogy and geochemistry of the pyrite stratiform deposit (e.g., Migaszewski and Gałuszka, 2019, 2023a, b; Migaszewski et al., 2023). However, little attention was given to pyrite framboids in the context of their provenance and relationship with other ore mineral occurrences. Hence, this study centres on the morphology and geochemistry of the framboidal pyrite. We have employed the arsenic, and partly cobalt and Co/Ni ratio, fingerprints to distinguish microbially-generated pyrite framboids from hydrothermal pyrite grains and veinlets. This study also fills the gap regarding the occurrence and provenance of pyrite framboids and associated pyrite microcrystals in the sediment-hosted hydrothermal pyrite deposits. This geochemically diverse environment gives a unique opportunity to look into the two pathways of pyrite formation in the context of multi-stage hydrothermal activity.

MATERIALS AND METHODS

OUTLINE OF GEOLOGICAL SETTING AND PYRITE MINERALIZATION

The study area is located north of the uptown section of Kielce, the capital city of the Holy Cross Mountains region (Fig. 1). This site occupies the Wiśniówka massif (elevation of 455.7 m a.s.l.) located in the western part of the Main Range. The massif is made up of Upper Cambrian (Lower Furongian) siliciclastic rocks assigned to the informal regional lithostratigraphic unit called the “Wiśniówka Sandstone Formation” (Orłowski, 1975). This formation consists mainly of alternating quartzite, quartzitic sandstone/siltstone and clayey-silty shale beds with subordinate bentonite and tuffite interlayers dipping northwards (Jaworowski and Sikorska, 2006; Żylińska et al., 2006; Migaszewski and Gałuszka, 2019). The black to dark grey pyritiferous sandstone-shale-bentonite beds predominate in the southern part of the Wiśniówka massif (Podwiśniówka), representing the oldest part of the geological section. There are three quarries in the study area (from west to east): (i) the historic Wiśniówka Mała (WM) quarry, now filled with a bipartite lake, (ii) the operational Wiśniówka Duża (WD) quarry, and (iii) the operational Podwiśniówka (Pw) quarry. Quarrying for quartzites has exposed pyritiferous rock beds in the last two open pits (Fig. 1).

Geochemical and mineralogical study of the rock succesion by Migaszewski and Gałuszka (2019) enabled the distinguishing of two stratiform (sediment-hosted hydrothermal) pyrite mineralization zones of different stratigraphic positions (from the south to the north): (i) Podwiśniówka (lowest Upper Cambrian) and (ii) Wiśniówka Duża (early-middle Upper Cambrian). The pyrite mineralization is confined only to the Wiśniówka Sandstone Formation and does not occur in the subjacent quartzite-bentonite/tuffite succession (Migaszewski and Gałuszka, 2019). The high concentrations of pyrite, generally uncommon in hard rock mining worldwide, have been observed especially in the Podwiśniówka area, giving rise to acid mine drainage (e.g., Migaszewski et al., 2008, 2018a, b, 2019).

Pyrite microcrystals are associated with goethite/hematite, REE-bearing minerals (goyazite, gorceixite and xenotime with

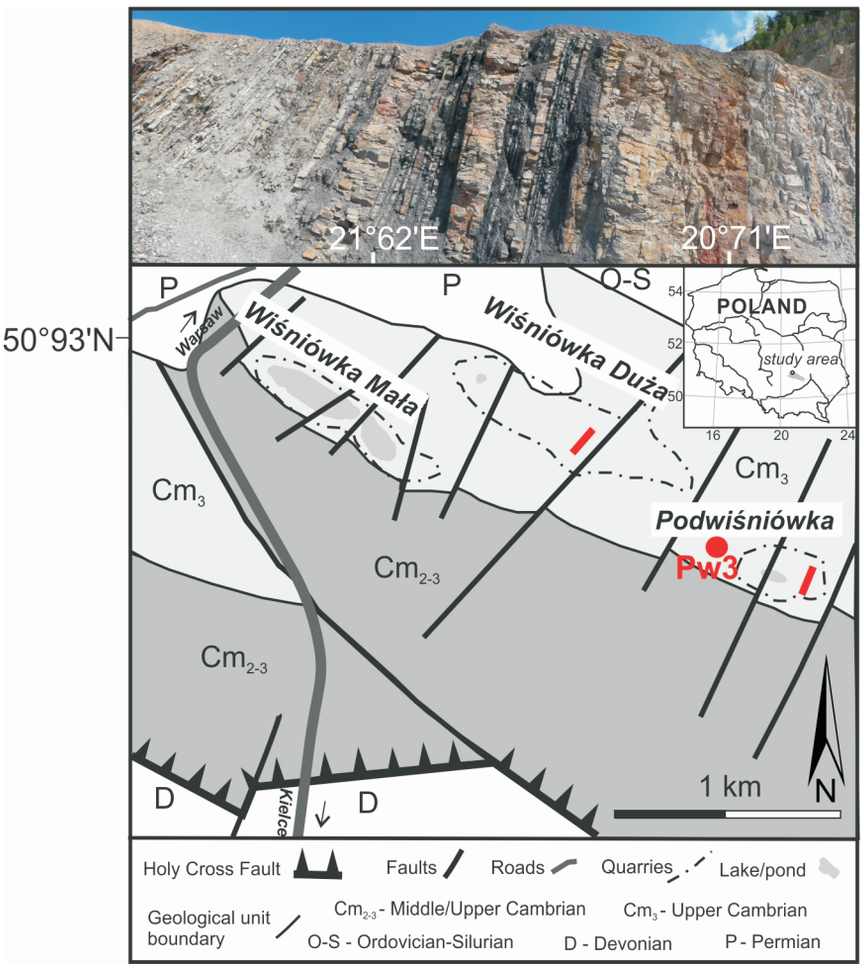

Fig. 1. Geological sketch map of the Wiśniówka acid mine drainage (AMD) area (modified after Żylińska et al., 2006) with location of borehole Pw3 and open pit walls sampled (marked in red)

subordinate monazite, crandallite and florencite), TiO_2 polymorphs (anatase, rutile, mixed rutile-anatase and rare rutile-brookite phases, and brookite), and nacrite. The other hydrothermal minerals, e.g., marcasite, galena, sphalerite, tetrahedrite, chalcopyrite, chalcocite, covellite, bornite, cinnabar, argentite, scorodite, barite, Fe-alloys mixed with other metals, chromite, and part of the zircon (besides the dominant detrital zircon), generally occur in trace amounts as tiny inclusions in pyrite microcrystals, goethite and TiO_2 polymorphs or in the rock matrix (e.g., Migaszewski et al., 2019, 2023; Migaszewski and Gałuszka, 2023a, b). All these mineral assemblages occur in the form of disseminated grains or aggregates mostly parallel to bedding, which is characteristic of sedimentary-exhalative (SEDEX)-type ore deposits (Leach et al., 2005; Qiu et al., 2018). Of particular interest are occasional quartzite-pyrite and quartzite-barite stratiform breccias or quartz sandstones cemented with pyrite which were formed in a Late Cambrian sedimentary basin. Hydrothermal index minerals (pyrite, nacrite, goyazite, gorceixite, xenotime, goethite/hematite) are indicative of crystallization temperatures in the range of 150–300°C (Migaszewski and Gałuszka, 2023b).

FIELDWORK AND SAMPLING

Geological fieldwork (profiling and sampling) has been performed since 2014 as quartzite mining progressed in the Podwiśniówka and Wiśniówka Duża quarries (Fig. 1). For the purpose of this study, 36 mineralized rock samples (weighing 0.5–1.0 kg each) were collected from exposed walls for more detailed mineralogical and geochemical study. Each sample was placed in a labelled polyethylene bag to prevent accidental mixing. During sampling, transport, storage and treatment, precautions were taken to avoid accidental contamination.

MICROSCOPE STUDY AND GEOCHEMICAL MICROANALYSIS

The rock samples were used for making epoxy-bound polished thin-sections to examine pyrite occurrences with optical microscopy in transmitted and reflected light using a polarizing microscope, model *Nikon Eclipse LV 100 Pol*. In all, 27 thin sections were carbon-coated for more detailed morphological and

microtextural characterization and imaging of framboidal and crystalline pyrite with scanning electron microscopy combined with energy-dispersive spectrometry (SEM-EDS), employing a model *LEO 1430* with an *EDS ISIS* Detector (Oxford Instruments Ltd.). For the purpose of this study, the following parameters were applied: signal A – backscattered electron (BSE), magnification 2.40–16.36 K×, acceleration voltage (EHT) 20 keV, working distance (WD) 10–12 mm.

Of the total of 27, 16 thin-sections (Pw1, Pw2, Pw3, Pw32, Pw33, Pw34, Pw35, Pw36, Pw38, Pw39, Pw40, Pw42, Pw3/11.5-11.6, Pw3/14.5-14.6, Pw3/81.1-81.2, WD6) were subject to electron microprobe analysis (EMPA), using a model *Cameca SX-100* equipped with five wavelength dispersive spectrometers. EHT was set at 15 keV, beam current at 20 nA, beam spot diameter at 1 to 5 mm in the BSE mode, counting times were 20 s on peak and 10 s on background. Standard materials included orthoclase $K[AlSi_3O_8]$, elemental As, skutterudite $CoNiAs_3$, chalcopyrite $CuFeS_2$, pentlandite $(Ni,Fe)_9S_8$, InSb and ZnSe. The main objective of the EMPA study was to analyse pyrite framboids, including all material that is present between the component microcrystallites, and the accompanying pyrite microcrystals for concentrations of As, Co, Cu, Ni, Sb, Se and Zn.

The basic petrographic study was conducted at the Environmental Analytical Laboratory, Jan Kochanowski University in Kielce whereas the SEM-EDS and EMPA investigations were performed at the Microanalysis Laboratory of the Polish Geological Institute – National Research Institute (PGI-NRI) in Warsaw. The microanalytical data obtained were processed using Microsoft® Excel for computing median values of the elements determined and the Co/Ni ratio in pyrite. The median values have not been calculated for elements below detection limits, i.e., 0.015 wt.% (censored) exceeding 20% of the total number of measuring points.

RESULTS AND DISCUSSION

MORPHOLOGY OF THE PYRITE FRAMBOIDS

In the Wiśniówka geological profile, pyrite microcrystals, aggregations and veinlets predominate over different forms of pyrite framboids. Results of EMP analysis show that the molar Fe/S ratio is 1 : 2 indicating that all these occurrences are represented by an iron disulphide, i.e., pyrite with scarcely any marcasite as indicated by a polarizing microscope study (data not shown). Framboids, likewise REE-minerals and TiO_2 polymorphs, occur primarily within dark grey to black carbonaceous clayey-silty shales and bentonites, especially in the Podwiśniówka geological section. These rock types prevail in the oldest (southern) strata that crop out in the Podwiśniówka area. Interestingly, pyrite crystals and veinlets, which are typically devoid of organic imprints, are distinctly abundant in quartzites and quartzitic sandstones/siltstones of the study area (Migaszewski and Gałuszka, 2019). Nearly all framboids are pyritic (Figs. 2A–G, 3 and 4), and their non-pyritic equivalents made up solely of primary iron oxy(hydr)oxides are extremely scarce (Fig. 2H).

There are two principal morphological types of framboidal pyrite: (i) isolated spherical or ellipsoidal framboids (Figs. 2 and 4B), and (ii) irregular aggregations (polyframboids, Figs. 3 and 4A, C, E). They occur predominantly as separate accumulations infilling rock matrix microvoids or interlaminar spaces/joints, occasionally within massive pyrite aggregations (Figs. 2A, E–G and 4D). These two different microtextural forms show diverse geochemistry that may throw light on their origin (discussed in the GEOCHEMISTRY OF THE PYRITE FRAMBOIDS subsection). Individual framboids typically range from 4 to 70 μm in diameter. Each individual framboid consists of loosely- or closely-packed (mostly with barely identified boundaries), equidimensional, equimorphic, locally multifaceted, nano- and microcrystallites (nano- and microglobules) varying from tens of nanometres to 1.5 μm in size, sporadically reaching even 10 μm across in some forms which underwent recrystallization into polygons. Some individual framboids reveal welded crystallites in their centre and loosely-packed crystallites in their outer parts (Fig. 2D).

Another interesting form, which may suggest its organic origin, is a cemented framboid surrounded by a chain of oval-shaped microcrystallites (Figs. 2A and 3A). These microcrystallites may represent authigenic pyrite encrustations on microbial cells, and thus reflect metabolic activity (Krajewski et al., 1994; Mozer, 2010). Some framboids have a spider-web matrix binding individual microcrystallites (Fig. 4B), which may have been formed within a low-temperature microbial biofilm (MacLean et al., 2008). The high-resolution SEM-EDS study excludes formation of such a matrix by the growth of individual framboidal microcrystallites within organic matter or clay (e.g., Cai et al., 2024). Nonetheless, in most recrystallized forms, this spider-web-like matrix underwent disappearance at the expense of enlarged microcrystallites. No single annular framboids lacking inner solid spaces have been observed in the samples examined. Some framboids contain single or double aureoles (cortices) composed of pyrite microcrystals resembling a flower calyx (”sunflower” according to Kosacz and Sawłowicz, 1983; Fig. 2G). This may suggest that some framboids may have served as nuclei for subsequent outward pyrite growth (Wilkin and Barnes, 1997), representing two different pathways of pyrite formation, i.e., pyritic framboids and pyrite microcrystals.

In places, single framboids show etching of their outer parts that may result from the recent oxidation of pyrite that triggers acid mine drainage formation (Fig. 4B). Some pyrite framboids are so densely packed that their inner original microtexture is partly or even totally obliterated (Figs. 2G, 3H and 4C–E). Notably, these forms, encapsulated in a pyrite matrix, locally reveal corroded boundaries that may suggest etching of framboidal surfaces induced by inputs of subsequent hydrothermal Fe(II)- and H_2S-bearing fluids (Figs. 2G and 4D). Microtextural interrelationships between these two different morphological pyrite forms may also indicate that framboids grew under sedimentary and early diagenetic conditions, thus excluding an impact of late diagenetic or epigenetic processes on their formation.

By contrast, agglomerations of different framboids attain 150 μm in size, typically showing composite microtextures made up of several individual framboids of different diameters and additionally composed of crystallites showing diverse shapes and sizes (Figs. 3 and 4A). In addition, these crystallites are loosely or densely packed within the same aggregations (Fig. 3H). Another characteristic feature of the Wiśniówka pyrite framboids, which may indicate their provenance, is a lack of mineral inclusions or different paragenetic associations of hydrothermal minerals (goethite/hematite, goyazite, xenotime, gorceixite, monazite, TiO_2 polymorphs, nacrite, metal sulphides, barite) as opposed to those found in the predominant pyrite microcrystal accumulations. By contrast, most pyrite crystals commonly show an oscillatory-zoned microtexture, i.e., the presence of alternating internal light grey (As-rich) and grey/dark grey (As-depleted) microbands that point to multi-stage inputs of hydrothermal fluids during their crystallization (Migaszewski et al., 2018a; Migaszewski and Gałuszka, 2019).

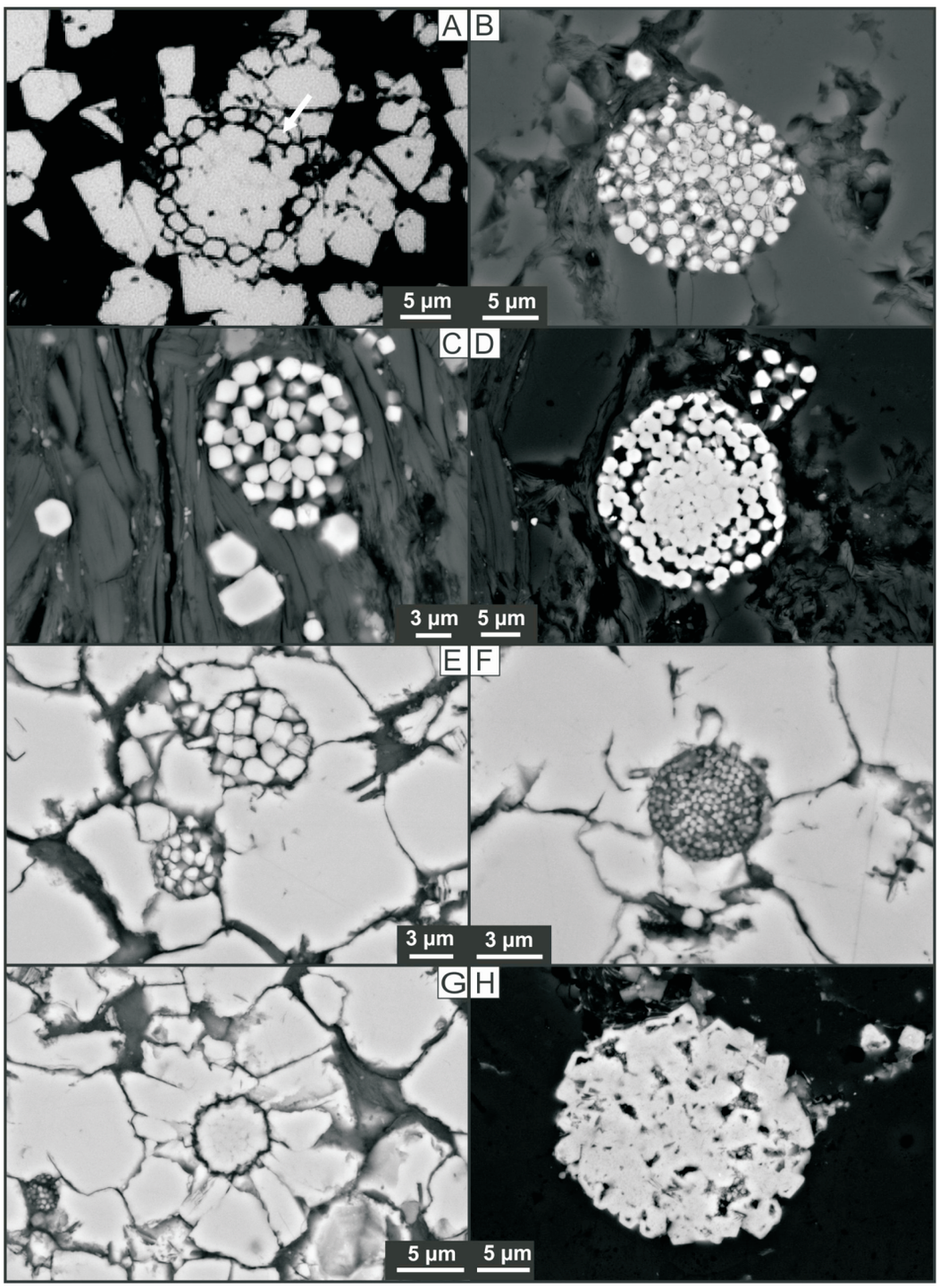

Fig. 2. Optical (reflected- and plane-polarized light) (A) and back-scattered SEM (B–H) photomicrographs of individual framboids

A – a cemented spherical pyrite framboid with a chain of microcrystallites (marked with white arrow) surrounded by pyrite euhedra (sample Pw3); **B** – a spherical framboidal pyrite aggregate made up of microcrystallites with a partly preserved pyritized spider-web matrix (sample Pw39); **C** – a loosely-packed spherical pyrite framboid associated with scattered pyrite euhedra that may be recrystallized former framboids (drill core sample Pw3/81.1-81.2); **D** – a spherical pyrite framboid composed of loosely-packed microcrystallites in the central part with a preserved pyritized spider-web matrix (drill core sample Pw3/81.1-81.2); **E** – three spherical pyrite framboids encapsulated in a pyrite microcrystal matrix (sample Pw33); **F** – a spherical pyrite framboid composed of nanocrystallites embedded in a pyrite microcrystal matrix (sample Pw33); **G** – an etched densely-packed pyrite framboid with overgrown pyrite crystals resembling a flower calyx (sample Pw33); **H** – a Fe-oxy(hydr)oxide framboid in a microvoid composed of loosely-packed microcrystallites (drill core sample Pw3/11.5-11.6)

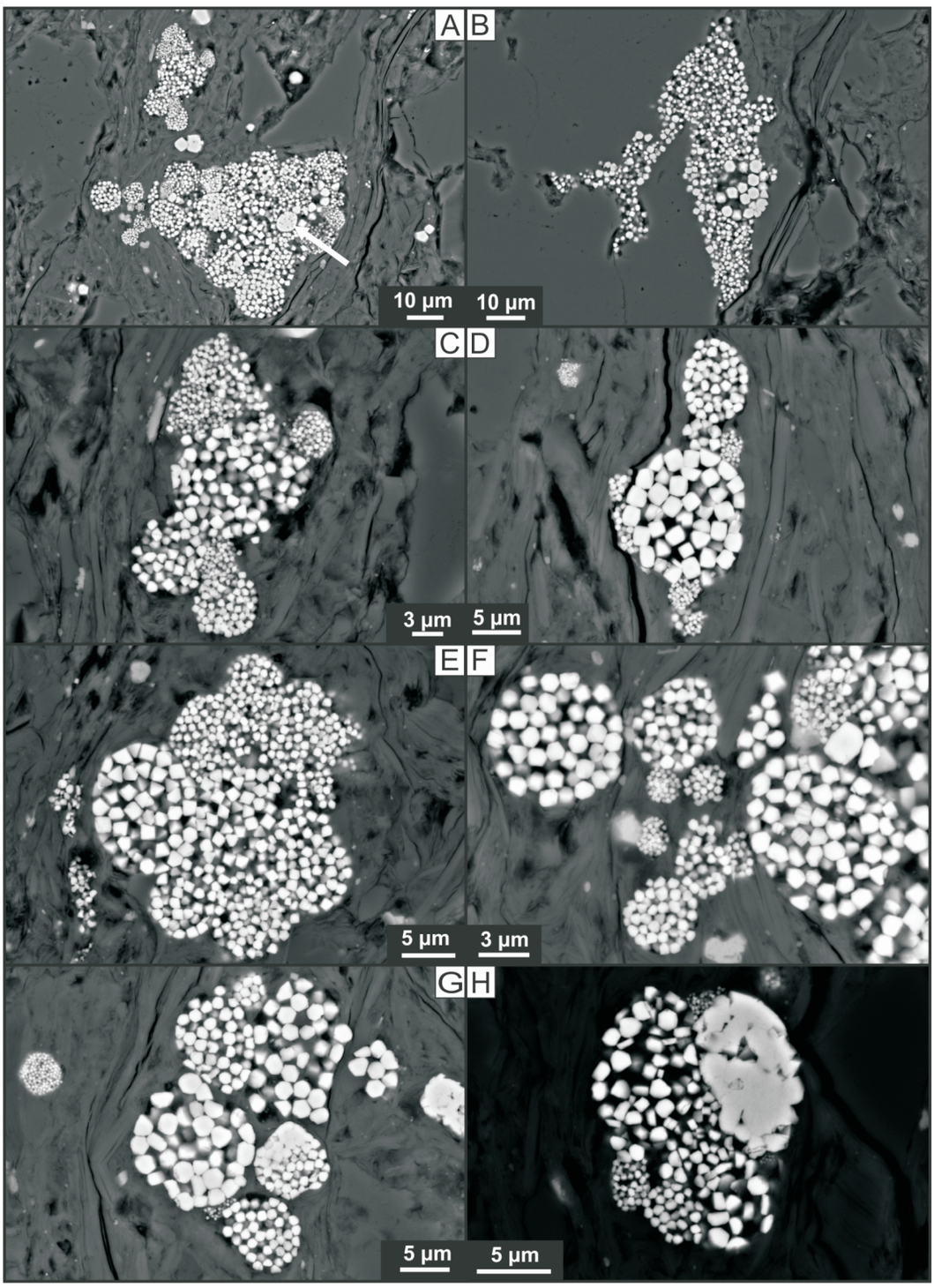

Fig. 3. Back-scattered SEM photomicrographs of framboidal pyrite aggregations

A – two densely-packed aggregations, each made up of different-sized and loosely-packed individual framboids; one framboid is surrounded by a chain of microcrystallites (marked with white arrow) (drill core sample Pw3/81.1-81.2); **B** – an irregular framboidal aggregation containing a framboid made up of larger loosely-packed crystallites (drill core sample Pw3/81.1-81.2); **C**–**F** – different-sized framboidal aggregations locally associated with pyrite euhedra (drill core sample Pw3/81.1-81.2); **G** – a pyrite aggregation composed of different-sized framboids (drill core sample Pw3/81.1-81.2); **H** – a closely-packed framboidal aggregation comprising a densely-packed recrystallized framboid (drill core sample Pw3/81.1-81.2)

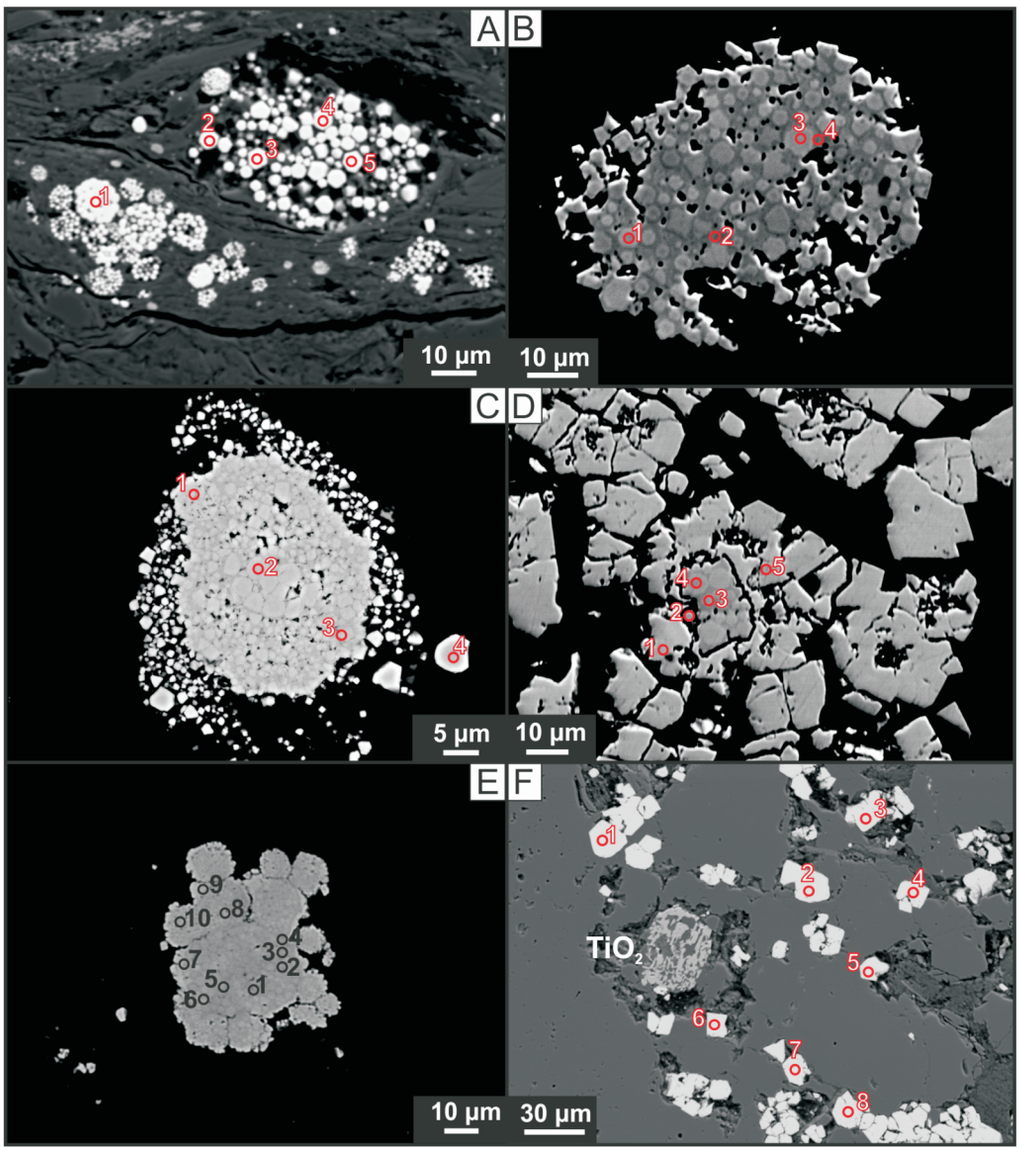

Fig. 4. Back-scattered SEM photomicrographs of pyrite occurrences with measuring points (see Table 2)

A – scattered different-sized pyrite framboids (drill core sample Pw3/81.1-81.2); **B** – an etched pyrite framboid revealing different-sized microcrystallites embedded in a spider-web-like matrix (sample Pw34); **C** – a composite framboid with a partly obliterated microtexture in the centre; different-sized microcrystallites embedded in a spider-web-like matrix (drill core sample Pw3/81.1-81.2); **D** – an etched framboid showing an obliterated microtexture, surrounded by pyrite microcrystals (sample Pw3); **E** – a framboid agglomeration with densely-packed microcrystallites (drill core sample Pw3/81.1-81.2); **F** – scattered pyrite euhedra associated with a TiO_2 polymorph grain (sample Pw38)

Another option that may be considered is oscillatory precipitation of As at the crystal/solution interface related to the As-concentration gradient in a single-stage solution.

GEOCHEMISTRY OF THE PYRITE FRAMBOIDS

Median and range concentrations of EMPA-determined metal(loid)s in the Wiśniówka pyrite are summarized in Table 1, while Table 2 shows the results of microanalysis performed on selected framboids. The corresponding measurement points of microanalysis are depicted in Figure 4. The results indicate that the pyrite framboids are distinctly depleted in arsenic (range of <0.015 to 0.43 wt.%) and antimony (<0.015 to 0.05 wt.%) compared to the dominant arsenical pyrite microcrystals. The latter contains an average of 1.92 wt.% As, attaining 6.33 wt.%, and even 8.23% As based on LA-ICP-MS measurements (Migaszewski and Gałuszka, 2019) and 3.66 wt.% Sb (Table 1). These high concentrations of As in pyrite microcrystals are unusual in sedimentary settings and are encountered only in hydrothermal veined metal-ore deposits, for instance, up to 4.5% in As-enriched pyrite of the Roudný gold deposit, Bohemian Massif (Zachariáš et al., 2004). The median contents of Cu and Zn in the framboids examined are 0.04 and 0.03 wt.%, respec-

Table 1

Median and range contents of metal(loid)s in pyrite framboids and microcrystals of the Wiśniówka area (based on EMP measurements)

Element	Pyrite framboids (n = 78)	Pyrite microcrystals (n = 93)
	[wt.%]	
As	<0.015–0.43	1.92 (0.06–6.33)*
Co	0.09 (<0.015–0.35)	<0.015–0.16
Cu	0.04 (<0.015–0.18)	<0.015–3.20
Ni	0.03 (<0.015–0.23)	0.02 (<0.015–0.31)**
Sb	<0.015–0.05	<0.015–3.66
Se	<0.015–0.04	<0.015–0.07
Zn	0.03 (<0.015–0.09)	<0.015–0.12

Median contents are not calculated for elements below detection limits (censored) exceeding 20% of the total number of measuring points

* – maximum content of 8.23% As was determined by LA-ICP-MS (Migaszewski and Gałuszka, 2019)

** – maximum content of Ni (13.3 wt.%) was measured by SEM-EDS; Ni substitutes for Fe in the pyrite crystal structure

tively, whereas the selenium content is below detection limits, i.e., 0.015 wt.%.

Of the other elements, contents of Co and Ni in the pyrite framboids vary from <0.015 to 0.35 wt.% and from <0.015 to 0.23 wt.% with a median value of 0.09 and 0.03 wt.%, respectively. The abundance of Co is in turn reflected by a higher Co/Ni ratio of median values averaging 3. A ratio value of <1 points to diagenetic pyrite origin, for example, in pre-ore framboidal pyrite of the Qixiashan Pb-Zn-Ag polymetallic deposit (Eastern China). The median concentrations of Co and Ni were 5.70 and 13.2 ppm (mg/kg), respectively, and the Co/Ni ratio amounted to 0.43 (Zhang et al., 2022). By contrast, Wiśniówka pyrite microcrystals display similar Ni contents (medium of 0.02 wt.%), but distinctly lower Co abundances (mostly <0.015 wt.%; Table 1).

Results of microanalysis suggest that a higher Co/Ni ratio, like depletion of As, may point to a negligible direct impact of hydrothermal processes on the growth of framboids, for example, one of these occurrences (Table 2 and Fig. 4C) is depleted in As (<0.015 wt.%), and slightly enriched in Co (0.02–0.18 wt.%), Cu (0.02–0.16 wt%), Ni (0.02–0.10 wt.%) and Zn (0.03–0.07 wt.%). Although its microtexture is obliterated, the lack of hydrothermal impact is also documented by the Co/Ni ratio varying from 1.8 to 6 (measuring points 1 through 3). The same relationship was also noted in densely-packed framboidal aggregations (Table 2 and Fig. 4E). The arsenic content ranges from <0.015 to 0.43 wt.%, whereas the Co/Ni ratio averages 1.8 with a range of 0.6 to 12. The other selected framboids contain commonly higher contents of Ni than Co (Table 2 and Fig. 4A, B, D), which may indicate an influence of subsequent hydrothermal fluids. This is also indicated by somewhat higher concentrations of arsenic in some framboids.

By contrast, pyrite microcrystals (Table 2 and Fig. 4F) show a distinct enrichment of As (range of 0.80 to 2.31 wt.%) and a dominance of Ni over Co (0.02 to 0.04 vs. <0.015 wt.%). The difference between these two pyrite types is particularly enhanced when it comes to comparing the contents of As in framboids with their pyrite microcrystal overgrowths (Table 2 and Fig. 4D). A densely-packed and corroded framboid contains 0.03 to 0.08 wt.% As (points 1, 2, 3 in Fig. 4D) whereas the surrounding aureole of pyrite grains shows a far higher abundance of this metalloid in the range of 0.92 to 2.44 wt.% (points 1, 5). This contrasts with results of the pyrite study from the upper oceanic crust of the South China Sea Basin, where framboidal pyrite is enriched in As and other trace elements compared to pyrite euhedra (Hu et al., 2022). Similarly, pyrite-filled cellular occurrences from Kentucky coals have been enriched in As up to 0.647% (Diehl et al., 2012). This means that this relationship varies from site to site depending on different environmental conditions.

Taken together, depletion of arsenic may be regarded as the Ariadne's web for the Wiśniówka framboids. Notably, somewhat higher As levels (range of 0.06 to 0.14 wt.%) were recorded in a pyritiferous framboidal template infilling spaces between microcrystallites (points 2 and 4 in Fig. 4B). By contrast, the content of As in microcrystallites is markedly lower, amounting to 0.02 and 0.03 wt.% (points 1 and 3 in Fig. 4B). For comparison, pyrite framboids from the recent Achterwasser lagoon sediments (western estuary of the Odra River, close to the German/Polish border) also contain low concentrations of arsenic, scarcely reaching 0.11 wt.% (Neumann et al., 2013).

FRAMBOIDAL PYRITE PROVENANCE

Studying framboids in stratiform pyrite deposits yields us an opportunity to figure out their organic origin. Wiśniówka stratiform mineralization zones are characterized by the presence of dominant sediment-hosted hydrothermal pyrite typically enriched in numerous metal-bearing minerals that may be employed to fingerprint different geological processes. Another signature of hydrothermal activity in the Wiśniówka Late Cambrian sedimentary basin is an unusual light sulphur enrichment of pyrite highlighted by a $\delta^{34}S$ range of –41.4 to –23.6‰ (Migaszewski and Gałuszka, 2019). These strongly negative $\delta^{34}S$ values were produced by reaction of hydrothermal Fe(II) with bacterially-reduced sulphur species (Boyce et al., 1983). Interestingly, framboids do not occur in the subjacent light grey quartzite-bentonite/tuffite succession exposed in the southeasternmost section of the Podwiśniówka quarry close to the Middle/Upper Cambrian boundary (Fig. 1). This implies that a lack of hydrothermal activity did not favour the formation of framboids and pyrite microcrystals at that time. All this changed with the deepening of the sedimentary basin combined with periodic sea-floor venting giving rise to the euxinic-anoxic environment. In order to unravel the provenance of the pyrite framboids and pyrite microcrystals, we must consider the specific morphology, microtexture, mineralogy and geochemistry of these two different mineral occurrences, that reflect diverse physicochemical conditions.

Framboidal pyrite morphology may be interpreted as a result of BSR activity that enabled rapid nucleation from fluids supersaturated with ferrous iron and hydrogen sulphide (Rickard, 2021). Both the microcrystal morphology and microtextural features of pyrite framboids *versus* pyrite microcrystals devoid of organic imprints, as well as the spatial relationships between these two pyrite types, point to their formation under sedimentary-early diagenetic conditions (Migaszewski and Gałuszka, 2019, 2023b), which has also been documented by other studies (e.g., Butler and Rickard, 2000; Folk, 2005). These framboids remained largely unaffected by late diagenetic and epigenetic processes, which is generally substantiated by the good

Table 2

Concentrations of metal(loid)s (in wt.%) in selected pyrite framboids (Pw3; 81.1–81.2 m, Pw3, Pw34, WD6) and pyrite microcrystals (Pw38) of the Wiśniówka mining area (based on EMP measurements)

Element	Pw3/81.1-81.2 [m] (Fig. 4A)					Pw34 (Fig. 4B)				Pw3/81.1-81.2 [m] (Fig. 4C)				Pw3 (Fig. 4D)				
	1	2	3	4	5	1	2	3	4	1	2	3	4	1	2	3	4	5
As	0.05	0.04	0.02	0.05	0.02	0.02	0.14	0.03	0.06	<	<	<	<	2.44	0.08	0.07	0.03	0.92
Co	<	<	<	<	<	<	<	<	<	0.18	0.06	0.15	0.02	<	0.02	0.02	<	<
Cu	0.02	<	<	0.02	<	<	0.02	<	0.05	0.14	0.16	0.08	0.02	0.05	<	0.03	<	<
Ni	0.02	0.02	0.04	0.02	0.03	0.02	0.04	0.02	0.07	0.10	0.02	0.08	0.03	0.05	0.02	0.05	<	<
Sb	0.03	<	0.03	0.02	0.02	<	0.02	0.03	<	<	0.02	<	0.02	<	<	0.05	<	0.02
Se	0.02	0.03	<	<	<	0.02	<	<	<	<	<	<	<	0.03	<	0.02	<	0.02
Zn	<	<	0.02	0.03	<	0.02	0.02	0.05	<	0.07	0.03	0.06	0.05	0.03	0.04	0.02	<	0.04

Tab. 2 cont.

Element	Pw3/81.-81.2 [m] (Fig. 4E)										Pw38 (Fig. 4F)							
	1	2	3	4	5	6	7	8	9	10	1	2	3	4	5	6	7	8
As	<	0.04	<	<	<	0.06	0.43	0.04	0.04	0.03	0.80	2.20	2.31	1.15	1.09	1.92	0.82	1.70
Co	0.12	0.22	0.19	0.21	0.06	0.13	0.30	0.11	0.18	0.19	<	<	<	<	<	<	<	<
Cu	0.04	0.07	0.09	0.10	0.04	0.07	0.07	0.09	0.04	0.11	0.02	0.02	0.02	<	<	<	<	<
Ni	0.02	0.06	0.05	0.05	0.10	0.09	0.23	0.05	0.18	0.11	0.02	0.02	0.02	0.03	0.04	0.03	0.02	0.04
Sb	0.02	0.02	<	0.05	0.03	<	<	<	<	0.02	0.04	<	0.22	0.02	0.04	0.06	0.02	<
Se	<	<	<	<	0.02	<	<	<	<	<	<	<	0.02	<	0.02	<	<	<
Zn	0.03	0.07	0.02	<	0.07	0.03	<	<	0.02	0.05	0.06	0.02	0.04	<	0.06	0.02	<	0.03

< – below 0.015 wt.%

state of their microtextural preservation. This was presumably induced by their incubation within black/dark grey carbonaceous clayey-silty shales and hydrothermal bentonites representing euxinic-anoxic facies. Some framboids show a well-preserved pyritized spider-web-like matrix (organic biofilm) with embedded nano- and microcrystallites (Fig. 4B this study; see also MacLean et al., 2008: Fig. 2C). This matrix now consists of pyrite that replaced microbially-formed organic matter (OM). The organic template in this biofilm represented a microenvironment that favoured both nucleation and growth of pyrite crystallites. This suggests their organic origin and excludes the direct formation of framboidal pyrite from solution within unconstrained microenvironments or free microvoids. Moreover, it is difficult to explain the diverse sizes of neighbouring individual framboids and their inner crystallites within composite aggregations (not to mention their co-occurrence with pyrite microcrystals) on the basis of inorganic processes. This means that nano- and microcrystallites of particular framboids may represent products of microbial activity locally slightly enlarged by the BSR process or recrystallized by consecutive inputs of hydrothermal fluids.

It should be stressed that the presence of larger framboids (above 5 or 6 mm across) does not point to their diagenetic or epigenetic origin, as indicated in other studies, for example by Wilkin et al. (1996) or Smolarek et al. (2014). The results of the present study also show that the size of framboids and their proportion to pyrite microcrystals cannot be used to discriminate euxinic-anoxic from suboxic-oxic conditions as observed in other depositional basins unaffected by hydrothermal processes (e.g., Wignall and Newton, 1998; Bond et al., 2004; Piper and Calvert, 2009; Smolarek et al., 2014). According to Wignall and Newton (1998), different-sized pyrite agglomerations are linked to the dimensions of bacterial occurrences and should not be used in the reconstruction of palaeoenvironmental redox conditions.

Aside from morphologic characteristics, the diverse chemical compositions of pyrite framboids and associated pyrite microcrystals also point to two different pathways of their formation. The depletion of trace elements (especially As) in pyrite framboids, suggests that the products of microbial activity formed between consecutive influxes of hydrothermal fluids into the sedimentary basin or as a result of their mixing with seawater at a distance from sea-floor vents. These hot metal(loid)- and H_2S-rich fluid inputs may have also inhibited the growth of framboids, triggering crystallization of pyrite microcrystals around framboid rims. The presence of sharp or corroded boundaries between framboids and pyrite overgrowths may suggest an impact of reactive, concentrated, high-temperature hydrothermal fluids (Figs. 2E–G and 4D).

However, a still unsolved issue is the contribution of hydrothermal fluids to the low-temperature BSR process that has been observed in many recent and fossil euxinic-anoxic environments (e.g., Wilkin and Barnes, 1997; Habicht and Canfield, 1997; Goldhaber, 2003; Mozer, 2010). In most sedimentary en-

vironments, sulphate-reducing bacteria metabolize at a temperature range of 0 to 80°C, but above this upper limit the BSR process ceases (Machel, 2001; Canfield et al., 2006; Sawicka et al., 2012). However, results of the earlier radiotracer study performed by Jørgensen et al. (1992) have revealed that sulphate reduction in deep-ocean sediments can take place at a temperature of up to 110°C, with an optimum range of 103 to 106°C. Paradoxically, the presence of hydrothermal minerals (As-rich pyrite, goethite/hematite, REE-minerals, TiO_2 polymorphs, nacrite, metal sulfides, barite, chromite and partly zircon) in the Wiśniówka Upper Cambrian siliciclastic formation points to higher crystallization temperatures varying from 150 to at least 300°C (Migaszewski and Gałuszka, 2019, 2023a, b). This may suggest that periodic inputs of high-temperature hydrothermal fluids supplied H_2S, Fe, As, Co, Ni and other metal(loid)s to the water column. Some of these chemical species may have been selectively taken up by microorganisms. A part of H_2S in turn may have undergone oxidation to SO_4^{2-}, which was then mixed up with seawater sulphate. Variations in the temperature and chemistry of hydrothermal fluids, and in the spatial distribution and intensity of vent activity, may have led to increase in or cessation of growth of pyrite framboids. However, the lack of microtextural relationships between pyrite framboids and hydrothermal index minerals may indicate that the framboids originated at a temperature <110°C.

CONCLUSIONS

This study shows that both pyrite framboids and microcrystals formed in a hydrothermally-impacted, early diagenetic sedimentary environment, both within the water column and in SO_4^{2-}/Fe-rich sediment porewater. Their morphologies, microtextures and geochemical features suggest that framboids represent products of microbial activity that formed under relatively reducing conditions at low temperatures as a result of mixing of seawater with periodic influxes of metal(loid)- and H_2S-rich hydrothermal fluids. Crystallization of pyrite microcrystals may have occurred during the more intense multi-stage hydrothermal activity associated with temporary cessation of framboid growth. This suggestion is supported by the presence of corroded framboidal aggregates overgrown by pyrite microcrystals. Enrichments of As and Ni in some densely-packed or recrystallized framboids may point to the rapid impact of high-temperature hydrothermal fluids on microbial activity. In addition, the occurrence of As-rich pyrite rims, enveloping some individual framboids, may be fingerprints of intermittent cessation of microbial growth. The predominance of framboids in the lower part of the Wiśniówka Upper Cambrian profile may have been linked to supersaturation levels of H_2S/SO_4^{2-} and Fe in a dominant organic-rich clayey-silty sediment.

Acknowledgements. The authors are grateful to L. Giro of the Polish Geological Institute – National Research Institute for taking SEM photomicrographs and performing preliminary EDS analysis. We would like to extend the same thanks to J. Janeczek of the Institute of Earth Sciences, University of Silesia in Sosnowiec and Z. Sawłowicz of the Institute of Geological Sciences, Jagiellonian University in Kraków for their insightful comments that considerably improved the quality of the manuscript. This study was supported by the Jan Kochanowski University in Kielce, Poland (a research grant # SUPB.RN.23.255).

REFERENCES

Astafieva, M.M., Rozanov, A.Yu., Hoover, R.B., 2005. Framboids: their structure and origin. Paleontological Journal, **39**: 457–464.

Bond, D., Wignall, P.B., Racki, G., 2004. Extent and duration of marine anoxia during the Frasnian-Famennian (Late Devonian) mass extinction in Poland, Germany, Austria and France. Geological Magazine, **141**: 173–193; https://doi.org/10.1017/S0016756804008866

Boyce, A.J., Coleman, M.L., Russel, M.J., 1983. Formation of fossil hydrothermal chimneys and mounds from Silvermines, Ireland. Nature, **306**: 545–550; https://doi.org/10.1038/306545a0

Butler, I.B., Rickard, D., 2000. Framboidal pyrite formation via the oxidation of iron(II) monosulfide by hydrogen sulphide. Geochimica et Cosmochimica Acta, **64**: 2665–2672; https://doi.org/10.1016/S0016-7037(00)00387-2

Cai, X., Xia, W., Liu, Y., Liao, S., Zhang, L., Hu, W., Liu, L., Li, W., Zheng, F., 2024. Microscopic characteristics and geological significance of pyrite in shales of the Wufeng-Longmaxi formations, southeastern Chongqing, China. Energy Geoscience, **5**, 100285; https://doi.org/10.1016/j.engeos.2023.100285

Canfield, D.E., Olesen, C.A., Cox, R.P., 2006. Temperature and its control of isotope fractionation by a sulfate-reducing bacterium. Geochimica et Cosmochimica Acta, **70**: 548–561; https://doi.org/10.1016/j.gca.2005.10.028

Cavalazzi, B., Agangi A., Barbieri, R., Franchi, F., Gasparotto, G., 2014. The formation of low-temperature sedimentary pyrite and its relationship with biologically-induced processes. Geology of Ore Deposits, **56**: 440–452; https://dx.doi.org/10.1134/S107570151405002X

Chang, X., Liu, X., Wang, H., Zhuang, G., Ma, Z., Yu, J., Chen, J., 2022. Depositional control on the sulfur content and isotope of sedimentary pyrite from the southeast coast of China since MIS5. Frontiers in Marine Science, **9**, 1005663; https://doi.org/10.3389/fmars.2022.1005663

Clark, G.R. II, Lutz, R.A., 1980. Pyritization in the shells of living bivalves. Geology, **8**: 268–271; https://doi.org/10.1130/0091-7613(1980)8%3C268:PITSOL%3E2.0.CO;2

Diehl, S.F., Goldhaber, M.B., Koenig, A.E., Lowers, H.A., Ruppert, L.F., 2012. Distribution of arsenic, selenium, and other trace elements in high pyrite Appalachian coals: evidence for multiple episodes of pyrite formation. International Journal of Coal Geology, **94**: 238–249; https://doi.org/10.1016/j.coal.2012.01.015

Działak, P., Syczewski, M.D., Kornaus, K., Słowakiewicz, M., Zych, Ł., Borkowski, A., 2022. Do bacterial viruses affect framboid-like mineral formation? Biogeosciences, **19**: 4533–4550; https://doi.org/10.5194/bg-19-4533-2022

Folk, R.L., 1993. SEM imaging of bacteria and nannobacteria in carbonate sediments and rocks. Journal of Sedimentary Research, **63**: 990–999; https://doi.org/10.1306/D4267C67-2B26-11D7-8648000102C1865D

Folk, R.L., 2005. Nannobacteria and the formation of framboidal pyrite: textural evidence. Journal of Earth System Science, **114**: 369–374; https://doi.org/10.1007/BF02702955

Garcia-Guinea, J., Martinez-Frias, J., Gonzales-Martin, R., Zamora, L., 1997. Framboidal pyrites in antique books. Nature, **388**: 631; https://doi.org/10.1038/41677

Goldhaber, M., 2003. Sulfur-rich sediments. Treatise on Geochemistry, **7**: 257–288; https://doi.org/10.1016/B0-08-043751-6/07139-5

Gong, Y.M., Shi, G.R., Weldon, E.A., Du, Y.S., Xu, R., 2008. Pyrite framboids interpreted as microbial colonies within the Permian *Zoophycos spreiten* from southeastern Australia. Geological Magazine, **145**: 95–103; https://doi.org/10.1017/S0016756807003974

Graham, U.M., Ohmoto, H., 1994. Experimental study of formation mechanisms of hydrothermal pyrite. Geochimica et Cosmochimica Acta, **58**: 2187–2201; https://doi.org/10.1016/0016-7037(94)90004-3

Gregory, D., Meffre, S., Large, R., 2014. Comparison of metal enrichment in pyrite framboids from a metal-enriched and metal-poor estuary. The American Mineralogist, **99**: 633–644; https://doi.org/10.2138/am.2014.4545

Gregory, D.D., Kovarik, L., Taylor, S.D., Perea, D.E., Owens, J.D., Atienza, N., Lyons, T.W., 2022. Nanoscale trace-element zoning in pyrite framboids and implications for paleoproxy applications. Geology, **50**: 736–740; https://doi.org/10.1130/G49890.1

Habicht, K.S., Canfield, D.E., 1997. Sulphur isotope fractionation during bacterial sulphate reduction in organic-rich sediments. Geochimica et Cosmochimica Acta, **6**: 5351–5361; https://doi.org/10.1016/S0016-7037(97)00311-6

Hu, S.-Y., Wang, X.-C., Tian, L., Martin, L., Schoneveld, L., Barnes, S.J., Guagliardo, P., Ding, W., Rickard, W.D.A., 2022. Variability of sulfur isotopes and trace metals in pyrite from the upper oceanic crust of the South China Sea basin, implications for sulfur and trace metal cycling in subsurface. Chemical Geology, **606**, 120982; https://doi.org/10.1016/j.chemgeo.2022.120982

Itaya, Y., 2022. Distribution analysis and speciation of arsenic and selenium in soils containing framboidal pyrite. Journal of Material Cycles and Waste Management, **24**: 1343–1354; https://doi.org/10.1007/s10163-022-01409-6

Jaworowski, K., Sikorska, M., 2006. Łysogóry Unit (Central Poland) *versus* East European Craton – application of sedimentological data from Cambrian siliciclastic association. Geological Quarterly, **50**: 77–88.

Jørgensen, B.B., Isaksen, M.F., Jannasch, H.W., 1992. Bacterial sulfate reduction above 100°C in deep-sea hydrothermal vent sediments. Science, **258**: 1756–1757; https://doi.org/10.1126/science.258.5089.1756

Kamata, A., Katoh, M., 2019. Arsenic release from marine sedimentary rock after excavation from urbanized coastal areas: oxidation of framboidal pyrite and subsequent natural suppression of arsenic release. Science of the Total Environment, **670**: 752–759; https://doi.org/10.1016/j.scitotenv.2019.03.217

Kosacz, R., Sawłowicz, Z., 1983. Forma występowania pirytu framboidalnego w złożu miedzi na monoklinie przedsudeckiej (in Polish). Rudy i Metale Nieżelazne, **8**: 292–297.

Krajewski, K.P., Van Cappelen, P., Trichet, J., Kuhn, O., Lucas, J., Martín-Algarra, A., Prévôt, L., Tewari, V.C., Gaspar, L., Knight, R.I., Lamboy, M., 1994. Biological processes and apatite formation in sedimentary environments. Eclogae Geologicae Helvetiae, **87**: 701–745; https://doi.org/10.5169/seals-167475

Leach, D.L., Sangster, D.F., Kelley, K.D., Large, R.R., Garven, G., Allen, C.R., Gutzmer, J., Walters, S., 2005. Sediment-hosted lead-zinc deposits: a global perspective. Economic Geology, **100**: 561–608; https://doi.org/10.5382/AV100.18

Liu, K., Huang, F., Gao, S., Zang, Z., Ren, Y., An, B., 2022. Morphology of framboidal pyrite and its textural evolution. Evidence from the Logatchev area, Mid-Atlantic Ridge. Ore Geology Reviews, **141**, 104630; https://doi.org/10.1016/j.oregeorev.2021.104630

Love, L.G., 1971. Early diagenetic polyframboidal pyrite, primary and redeposited, from the Wenlockian Denbigh Grit Group, Conway, North Wales, U.K. Journal of Sedimentary Research, **41**: 1038–1044; https://doi.org/10.1306/74D723EC-2B21-11D7-8648000102C1865D

Lowers, H.A., Breit, G.N., Foster, A.L., Whitney, J., Yount, J., Uddin, M.N., Muneem, A.A., 2007. Arsenic incorporation into authigenic pyrite, Bengal Basin sediment, Bangladesh. Geochimica et Cosmochimica Acta, **71**: 2699–2717; https://doi.org/10.1016/j.gca.2007.03.022

Machel, H.G., 2001. Bacterial and thermochemical sulfate reduction in diagenetic settings – old and new insights. Sedimentary Geology, **140**: 143–175; https://doi.org/10.1016/S0037-0738(00)00176-7

MacLean, L.C.W., Tyliszczak, T., Gilbert, U.P.A., Zhou, D., Pray, T.J., Onstott, T.C., Southam, G., 2008. A high-resolution chemical and structural study of framboidal pyrite formed within a low temperature bacterial biofilm. Geobiology, **6**: 471–480; https://doi.org/10.1111/j.1472-4669.2008.00174.x

Migaszewski Z.M., Gałuszka A., 2019. The origin of pyrite mineralization: implications for Late Cambrian geology of the Holy Cross Mountains (south-central Poland). Sedimentary Geology, **390**: 45–61; https://doi.org/10.1016/j.sedgeo.2019.07.004

Migaszewski, Z.M., Gałuszka, A., 2023a. The use of rare earth element profiles as a proxy for a fractionation source and mine-waste provenance. Science of the Total Environment, **901**, 166517; https://doi.org/10.1016/j.scitotenv.2023.166517

Migaszewski, Z.M., Gałuszka, A., 2023b. Hydrothermal TiO_2 polymorphs in a pyrite stratiform deposit: lessons from a mineralogical and geochemical multiproxy record. Chemical Geology, **632**, 121551; https://doi.org/10.1016/j.chemgeo.2023.121551

Migaszewski, Z.M., Gałuszka, A., Hałas, S., Dołęgowska, S., Dąbek, J., Starnawska, E., 2008. Geochemistry and stable sulfur and oxygen isotope ratios of the Podwiśniówka pit pond water generated by acid mine drainage (Holy Cross Mountains, south-central Poland). Applied Geochemistry, **23**: 3620–3634; https://doi.org/10.1016/j.apgeochem.2008.09.001

Migaszewski, Z.M., Gałuszka, A., Dołęgowska, S., 2018a. Arsenic in the Wiśniówka acid mine drainage area (south-central Poland) – mineralogy, hydrogeochemistry, remediation. Chemical Geology, **493**: 491–503; https://doi.org/10.1016/j.chemgeo.2018.06.027

Migaszewski, Z.M., Gałuszka, A., Dołęgowska, S., 2018b. Stable isotope geochemistry of acid mine drainage from the Wiśniówka area (south-central Poland). Applied Geochemistry, **95**: 45–56; https://doi.org/10.1016/j.apgeochem.2018.05.015

Migaszewski, Z.M., Gałuszka, A., Dołęgowska, S., 2019. Extreme enrichment of arsenic and rare earth elements in acid mine drainage: case study of Wiśniówka mining area (south-central Poland). Environmental Pollution, **244**: 898–906; https://doi.org/10.1016/j.envpol.2018.10.106

Migaszewski, Z.M., Gałuszka, A., Zieliński, G., 2023. REE-bearing minerals in sediment-hosted stratiform pyrite mineralization zones of the Wiśniówka area (Holy Cross Mts., Poland). Geological Quarterly, **67**, 17; https://doi.org/10.7306/gq.1687

Mozer, A., 2010. Authigenic pyrite framboids in sedimentary facies of the Mount Wawel Formation (Eocene), King George Island, West Antarctica. Polish Polar Research, **31**: 255–272; https://doi.org/10.2478/v10183-010-0004-2

Mukherjee, I., Deb, M., Large, R.R., Halpin, J., Meffre, S., Ávila, J., Belousov, I., 2020. Pyrite textures, trace elements and sulfur isotope chemistry of Bijaigarh Shales, Vindhyan Basin, India and their implications. Minerals, **10**, 588; https://doi.org/10.3390/min10070588

Neumann, T., Scholtz, F., Kramar, U., Ostermaier, M., Rausch, N., Berner, Z., 2013. Arsenic in framboidal pyrite from recent sediments of a shallow water lagoon of the Baltic Sea. Sedimentology, **60**: 1389–1404; https://doi.org/10.1111/sed.12031

Ohfuji, H., Rickard, D., 2005. Experimental synthesis of framboids – a review. Earth-Science Reviews, **71**: 147–170; https://doi.org/10.1016/j.earscirev.2005.02.001

Orłowski, S., 1975. Cambrian and Upper Precambrian lithostratigraphic units in the Holy Cross Mts: (in Polish with English summary). Acta Geologica Polonica, **25**: 431–448.

Ostwald, J., England, B.M., 1979. The relationship between euhedral and framboidal pyrite in base-metal sulphide ores. Mineralogical Magazine, **43**: 297–300; https://doi.org/10.1180/minmag.1979.043.326.13

Paktunc, A.D., Davé, N.K., 2002. Formation of secondary pyrite and carbonate minerals in the Lower Williams Lake tailings basin, Elliot Lake, Ontario. American Mineralogist, **87**: 593–602; https://doi.org/10.2138/am-2002-5-601

Piper, D.Z., Calvert, S.E., 2009. A marine biogeochemical perspective on black shale deposition. Earth-Science Reviews, **95**: 63–96; https://doi.org/10.1016/j.earscirev.2009.03.001

Popa, R., Badescu, A., Kinkle, B.K., 2004. Pyrite framboids as biomarkers for iron-sulfur systems. Geomicrobiology Journal, **21**: 1–14; https://doi.org/10.1080/01490450490275497

Qiu, W.J., Zhou, M.-F., Li, X., Williams-Jones, A.E., Yuan, H., 2018. The genesis of the Giant Dajiangping SEDEX-type pyrite deposit, South China. Economic Geology, **113**: 1419–1446;

Rickard, D., 2021. Framboids. Oxford University Press. https://doi.org/10.1093/oso/9780190080112.001.0001

Rust, G.W., 1935. Colloidal primary copper ores in Cornwall Mines, southeastern Missouri. The Journal of Geology, **43**: 398–426; https://doi.org/10.1086/624318

Sawicka, J.E., Jørgensen, B.B., Brüchert, V., 2012. Temperature characteristics of bacterial sulfate reduction in continental slope and slope sediments. Biogeosciences, **9**: 3425–3435; https://doi.org/10.5194/bg-9-3425-2012

Sawłowicz, Z., 1993. Pyrite framboids and their development: a new conceptual mechanism. Geologische Rundschau, **82**: 148–156; https://doi.org/10.1007/BF00563277

Sawłowicz, Z., 2000. Framboids: from their origin to application. Prace Mineralogiczne, **88**.

Schieber, J., 2002. Sedimentary pyrite: a window into the microbial past. Geology, **30**: 531–534; https://doi.org/10.1130/0091-7613(2002)030%3C0531:SPAWIT%3E2.0.CO;2

Schopf, J.M., 1965. Fossil iron bacteria preserved in pyrite. Proceedings of the American Philosophical Society, **109**: 288–308.

Smolarek, J., Marynowski, L., Trela, W., 2014. Ordovician Jeleniów Claystone Formation of the Holy Cross Mountains, Poland – reconstruction of redox conditions using pyrite framboid study. Contemporary Trends of Geoscience, **3**: 59–67; https://doi.org/10.2478/ctg-2014-0023

Soliman, M.F., El Goresy, A., 2012. Framboidal and idiomorphic pyrite in the upper Maastrichtian sedimentary rocks at Gabal Oweina, Nile Valley, Egypt: formation processes, oxidation products and genetic implications to the origin of framboidal pyrite. Geochimica et Cosmochimica Acta, **90**: 195–220; https://doi.org/10.1016/j.gca.2012.05.004

Sugawara, H., Sakakibara, M., Belton, D., Suzuki, T., 2013. Formation process of pyrite polyframboid based on the heavy-metal analysis by micro-PIXE. Environmental Earth Sciences, **69**: 811–819; https://doi.org/10.1007/s12665-012-1966-7

Szczepanik, P., Sawłowicz, Z., Bąk, M., 2004. Pyrite framboids in pyritized radiolarian skeletons (Mid-Cretaceous of the Pieniny Klippen Belt, Western Carpathians, Poland). Annales Societatis Geologorum Poloniae, **74**: 35–41.

Ueshima, M., Hashimoto, Y., Sakanakura, H., 2019. Chemical stability of framboidal pyrite containing geogenic arsenic in alluvial sediments. Journal of Environmental Quality, **48**: 1907–1912. https://doi.org/10.2134/jeq2019.04.0174

Wang, P., Huang, Y., Wang, C., Feng, Z., Huang, Q., 2013. Pyrite morphology in the first member of the Late Cretaceous Qingshankou Formation, Songliao Basin, Northeast China. Palaeogeography, Palaeoclimatology, Palaeoecology, **385**: 125–136; https://doi.org/10.1016/j.palaeo.2012.09.027

Wignall, P.B., Newton, R., 1998. Pyrite framboid diameter as a measure of oxygen deficiency in ancient mudrocks. American Journal of Science, **298**: 537–552; https://doi.org/10.2475/ajs.298.7.537

Wilkin, R.T., Barnes, H.L., 1997. Formation processes of framboidal pyrite. Geochimica et Cosmochimica Acta, **61**: 323–339; https://doi.org/10.1016/S0016-7037(96)00320-1

Wilkin, R.T., Barnes, H.L. Brantley, S.L., 1996. The size distribution of framboidal pyrite in modern sediments: an indicator of redox conditions. Geochimica et Cosmochimica Acta, **60**: 3897–3912; https://doi.org/10.1016/0016-7037(96)00209-8

Zachariáš, J., Frýda, J., Paterová, B., Mihaljevič, M., 2004. Arsenopyrite and As-bearing pyrite from the Roudný deposit, Bohemian Massif. Mineralogical Magazine, **68**: 31–46; https://doi.org/10.1180/0026461046810169

Zhang, W.-D., Li, B., Lu, A.-H., Zhao, K.-D., Elatikpo, S.M., Chen, X.-D., Zhu, L., Yu, M., 2022. In-situ pyrite trace elements and sulfur isotope characteristics and metallogenic implications of the Qixiashan Pb-Zn-Ag polymetallic deposit, Eastern China. Ore Geology Reviews, **144**, 104849; https://doi.org/10.1016/j.oregeorev.2022.104849

Zhang, J., Liang, H., He, X., Yang, Y., Chen, B., 2011. Sulfur isotopes of framboidal pyrite in the Permian-Triassic boundary clay at Meishan section. Acta Geologica Sinica, **85**: 694–701; https://doi.org/10.1111/j.1755-6724.2011.00462.x

Żylińska, A., Szczepanik, Z., Salwa, S., 2006. Cambrian of the Holy Cross Mountains, Poland: biostratigraphy of the Wiśniówka Hill succession. Acta Geologica Polonica, **56**: 443–461.